SCIENTIFIC REPORTS

OPEN

SUBJECT AREAS:
MAGNETIC PROPERTIES AND MATERIALS
ELECTRONIC STRUCTURE

Received
17 July 2013

Accepted
8 November 2013

Published
3 December 2013

Correspondence and requests for materials should be addressed to B.S. (biplab.sanyal@physics.uu.se)

Defect controlled magnetism in FeP/graphene/Ni(111)

Sumanta Bhandary, Olle Eriksson & Biplab Sanyal

Department of Physics and Astronomy, Uppsala University, Box 516, 75120 Uppsala, Sweden.

Spin switching of organometallic complexes by ferromagnetic surfaces is an important topic in the area of molecular nanospintronics. Moreover, graphene has been shown as a 2D surface for physisorption of molecular magnets and strain engineering on graphene can tune the spin state of an iron porphyrin (FeP) molecule from S = 1 to S = 2. Our ab initio density functional calculations suggest that a pristine graphene layer placed between a Ni(111) surface and FeP yields an extremely weak exchange interaction between FeP and Ni whereas the introduction of defects in graphene shows a variety of ferromagnetic and antiferromagnetic exchange interactions. Moreover, these defects control the easy axes of magnetization, strengths of magnetic anisotropy energies and spin-dipolar contributions. Our study suggests a new way of manipulating molecular magnetism by defects in graphene and hence has the potential to be explored in designing spin qubits to realize logic operations in molecular nanospintronics.

The combination of spintronics and molecular electronics is a rapidly emerging research field due to the possibility of manipulating spin and charge degrees of freedom at the molecular scale. A key factor in molecular nanospintronics is the efficient control of electronic and magnetic properties of molecules acting as the active region of spin-dependent electronic transport. Metalorganics with a magnetic centre own a key position in this respect. The possibility of controlled spin manipulation[1–4] makes these magnets attractive for several device applications including spin-dependent electronics, molecular switches etc. In this regard, the use of materials that could be stabilized at an ultra thin atomic limit are a perfect choice for future devices, where graphene has already made its mark very significantly. Very recently, we have proposed[5] that strain engineering in a graphene lattice carrying a divacancy defect can switch the spin state of an iron porphyrin (FeP) molecule adsorbed on the defect site from S = 1 to S = 2 in a reversible way.

Graphene has been very much in the center of research interest in the last decade[6–8] and continues to be there as a potential key-material in electronics, storage materials, bio-sensors, DNA-sequencing, drug delivery and so on. It has also been proven promising in the area of bio-molecular devices. Free standing graphene with sp^2 bonded C atoms possess no magnetism but it can be introduced by either confinement[9], where unsaturated bond or electron localization plays the key role, or depositing on a magnetic surface[10], where substrate induced moment is observed. It should be noted that graphene is prone to several types of point defects, e.g., vacancies, Stone-Wales defects etc[11,12]. The influence of these defects in the induced magnetism in graphene is less explored in the literature, which may have important consequences in mediating exchange interactions via graphene. In this article, our objective is to explore magnetism in graphene adsorbed on a Ni(111) surface and utilize the possibility to achieve a control over magnetic interaction between Ni surface and organometallic molecule like iron porphyrin (FeP). The first part of our discussion thus will be devoted to magnetism in graphene including the effect of defects in the graphene lattice and in the later part we shall discuss magnetic interactions between FeP and magnetic Ni surface via graphene.

It has been shown that a magnetic surface with partially filled d-orbital favors chemisorption of molecular magnets[4]. Due to the formation of covalent bonds with the magnetic substrates, FeP is structurally deformed with enhanced Fe-N bond lengths compared to the gas-phase geometry, leading to a change in the spin state of Fe from the gas-phase value of S = 1 to a high spin-state S = 2 for the chemisorbed situation[4]. However, the presence of adsorbed graphene between FeP and magnetic substrates weakens both chemical and magnetic interaction due to physisorption of FeP on graphene. More importantly, as will be evidenced later, ferrimagnetism induced in graphene by the underlying Ni substrate in a peculiar sub-lattice pattern dictates the nature and strength of magnetic interaction between FeP and the Ni substrate whereas a free standing non-magnetic graphene or graphene deposited on non-magnetic substrates, such as Cu, Pt etc. acts inert in this respect. A complex scenario occurs in the presence of defects in graphene as this changes the induced magnetisation profile in the graphene lattice and hence the nature and strength of magnetic interaction. The primary focus of our study is the role of

defects viz. monovacancy, divacancy and Stone-Wales (SW) defects in manipulating intramolecular magnetism as well as molecule-substrate interactions. It should be stated that controlled introduction of defects in graphene has been realised recently[13,14], which, as we demonstrate here by first principles density functional calculations, opens up the possibility to manipulate magnetic interactions via these defects.

Results

Induced magnetism in pure and defected grapheme. A sp^2 -bonded graphene lattice has three in-plane saturated bonds along with an out-of-plane π-bond. The dispersive π-bonding (anti bonding) band appears just below (above) the Fermi energy. Once adsorbed on a hexagonal facet of Ni(111) surface, C atoms in one of the two sublattices make direct bonds with Ni atoms right underneath them, while the other sublattice C atoms stay hanging on the hexagonal centres of the top Ni layer. From now on, we indicate the C-atom, that makes direct bond with Ni, as C_A and the other sublattice C atoms as C_B. The calculated distance between the graphene layer and the Ni surface comes out to be 2.1 Å for defect free graphene, which agrees quite well with previous experimental[10] and theoretical[15] studies. Owing to the strong covalent interaction between Ni $-$ d_{z^2} and C_A -p_z orbitals, the C-p_z orbital is pushed down in energy, thus allowing the C_A sublattice to hybridize with the lower part of the Ni band in both majority and minority spin channels. The C-p_z orbital of the other sublattice of graphene interacts weakly with Ni $-$ d_{z^2} orbital through π-bonding and appears more close to the Fermi energy. A C_A atom gains a small moment of 0.018 μ_B with an opposite polarization compared to the Ni moment in the process of strong hybridization while a C_B atom acquires a comparatively larger moment of 0.029 μ_B with the same sign as the Ni moment. Hence, the whole graphene layer acquires the characteristic of a ferrimagnet with alternative sublattices having opposite spin polarizations as shown in Fig. 1(a). The total contribution in the defect-free graphene arising from C_B (36 atoms) is 1.025 μ_B and from C_A (36 atoms) is -0.651 μ_B where each C atom of a particular sublattice contributes equally. Due to these features of hybridization, the broad surface Ni band also gets divided into two sub-bands, of which one appear 2–4 eV below Fermi energy and the other appears close to Fermi energy (discussed below).

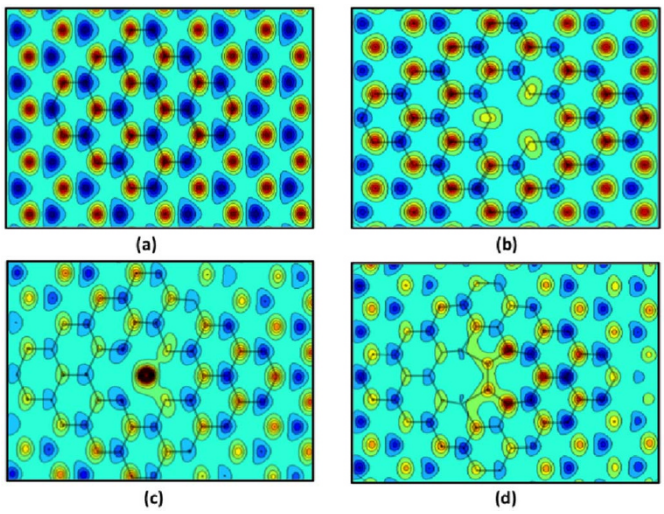

Figure 1 | Magnetization densities in the graphene lattice on Ni(111) (a) without any defect (b) with a monovacancy, (c) with a divacancy and (d) with a SW defect. Red and blue colors indicate positive and negative densities respectively.

Intricate magnetization profiles in the graphene lattice are observed with the introduction of lattice defects, as shown in Figs. 1(b)–(d). We have considered three types of defects, that are abundant in graphene, e.g. the monovacancy, where one C_A atom is removed, a divacancy, where a pair of C_A and C_B atoms are removed and Stone-Wales defect, where a C-bond is rotated by 90° to form a 5-5-7-7 structure. The following structural and magnetic changes are observed: (i) *monovacancy*: the graphene lattice with a monovacancy is magnetised almost in a similar fashion as the pristine graphene. Only at the defect site, the absence of one C_A atom (with moment of opposite polarization to Ni in the ideal honeycomb lattice) reduces the moments of the surrounding three C_B atoms to 0.016 μ_B as shown in Fig. 1(b); (ii) *divacancy*: to heal a divacancy defect in graphene, one Ni atom is lifted up towards the vacancy center leaving a void in the surface Ni layer as shown in the inset of Fig. 2. Due to the modified coordination and thus modified hybridization and ligand field, the spin moment of that particular Ni atom quenches to 0.04 μ_B. This local structural deformation is transmitted through the whole unit cell and hence, the induced moments in different C-atoms vary significantly due to strongly affected graphene-Ni interaction (Fig. 1(c)). This results in a decrease in total induced moments in both C-sublattices, amounting to 0.403 μ_B(35 atoms) and -0.165 μ_B(35 atoms); (iii) *SW*: compared to a divacancy defect, a SW defect center introduces more structural changes by mostly buckling the graphene lattice. The effective separation between the graphene layer and the Ni surface varies significantly in the unit cell (2.1 Å to 2.6 Å) for this defect and hence the induced magnetization in graphene varies from 0.003 to 0.03 μ_B. The sublattice magnetization profile shown in Fig. 1(d) depicts the situation with the differently polarized moments in the graphene lattice being 0.35 μ_B(39 atoms) and -0.17 μ_B(33 atoms). The buckling in the graphene lattice affects the C-Ni hybridisation, which has a direct impact on varying the magnetization on different C atoms. Therefore, one may conclude that the controlled introduction of specific lattice defects is a possible route to drastically modify the magnetization profile of the adsorbed graphene lattice on Ni.

Interaction between FeP and pristine grapheme. As mentioned earlier, a metallic magnetic surface promotes chemisorption of an organometallic molecule (FeP)[4] and hence a strong exchange interaction between Fe and the magnetic substrate. It would be desirable to be able to control this exchange interaction. We show

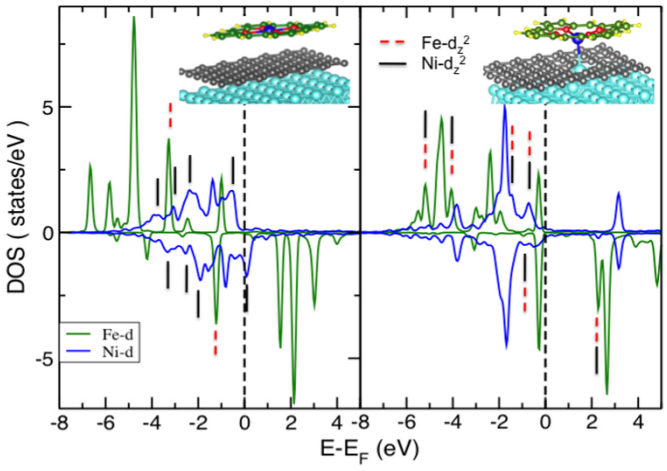

Figure 2 | Spin-polarized d-orbital projected density of states of Fe in FeP and the Ni atom occupying the divacancy site shown in the right panel for (left) graphene without defect and (right) graphene with a divacancy defect. The corresponding geometries with FeP/graphene/Ni are shown in the inset. The vertical bars indicate d_{z^2} character of Fe and Ni at different energy positions in the DOS.

here that a graphene layer placed between the magnetic surface and FeP blocks the path for strong exchange interaction between the magnetic molecule and the Ni substrate and at the same time the ferrimagnetic graphene opens up new paths of magnetic interaction between the magnetic center in the molecule and the magnetic surface.

The composite system, which we consider is FeP adsorbed on a graphene layer deposited on a Ni(111) surface. FeP becomes physisorbed on the crystalline graphene lattice or at defect centres in the graphene lattice. The average distance between FeP and graphene is calculated to be 3.1 Å and the graphene to Ni distance turns out to be 2.1 Å. Hence, the magnetic interaction with an effective distance of 5.2 Å is expected be an order or two weaker compared to the chemisorbed situation (without graphene) if only direct exchange is considered. From our calculations, we confirm this scenario where the variation in strength of the exchange energy enters due to different adsorption sites.

We now consider each adsorption site individually. We have considered three adsorption sites for pristine graphene, namely **Top-A**, **Top-B** and **Hexagon** positions, where the Fe centre of FeP is on top of C_A, C_B and in the center of a hexagonal ring, respectively. The magnetization profile for a defect free graphene layer has an alternative arrangement of oppositely polarized moments of the C bipartite lattice. The Fe atom of FeP placed on top of a hexagonal site has a vanishingly small exchange coupling with the Ni substrate whereas the binding energy (2.22 eV) is the highest for this adsorption site. The spin-state of Fe changes from the value of the free molecule, S = 1 to S = 2 for this most favorable adsorption site. A strong π-π stacking between the ring atoms of FeP and the π network in the graphene lattice gives rise to enhanced Fe-N bond lengths along with an overall outward expansion of FeP. Hence, a change of spin state occurs and the high spin state is stabilized.

Adsorption of FeP directly on the Ni surface leads to the formation of chemical bonds between FeP and Ni and hence establishes a fairly strong ferromagnetic exchange coupling between them[4]. The insertion of the graphene layer blocks the direct exchange between Fe and Ni significantly causing the magnetic coupling to be mediated in an indirect way. The local ligand field on Fe, predominantly provided by N atoms along with weaker contribution from the C-ring, affects the energy positions of the Fe-d orbitals. In-plane N-p_x and p_y orbitals hybridize strongly with Fe $-$ $d_{x^2-y^2}$ and push this level up in energy. The out-of-plane orbitals on N atoms provide a π-type bond with Fe-d_π orbital and hence push the d_π orbital above the d_{xy} orbital. We note in passing that the ligand field effects discussed here are influenced by the formation of molecular orbital states within the FeP molecule, which are influenced by the interaction with the graphene layer. Hence, these effects are different from the crystal field level splitting in a square planar point charge arrangement. Along with the $\pi - \pi$ interaction between Fe-d and N-p, C-p and N-p orbitals contribute to intramolecular hybridization in FeP. However, a much weaker hybridization is observed between FeP and graphene.

For the **Top-A** position, the Fe moment is antiparallel to the moment of C_A (-0.018 μ_B) and hence is parallel to the Ni moment, giving rise to a ferromagnetic exchange coupling of strength $\sim$1.8 meV between FeP and Ni. For the **Top-B** site, an antiferromagnetic exchange coupling (7 meV) between Fe and Ni is observed. Similar to the **Top-A** site, the spin-state of Fe is retained as S = 1. The binding energies of FeP on **Top-A** and **Top-B** sites are only 2 meV and 17 meV higher than the most favorable **Hexagonal** site, where a vanishingly small exchange coupling is observed.

Influence of defects. Now we discuss the role of defects in modifying the structural, electronic and magnetic properties. (i) On a monovacancy defect, Fe prefers to sit on top of the defect site giving rise to a ferromagnetic coupling energy of 7 meV between Fe and Ni. The spin state remains unaffected with S = 1. (ii) The situation differs quite significantly for a divacancy defect. One Ni atom from the substrate occupies the divacancy site and makes a strong chemical bond with Fe in FeP as shown in the inset of Fig. 2. As a result, the Fe atom is pulled towards the Ni atom from the plane of FeP stretching the Fe-N bond lengths. This changes the spin state from S = 1 to S = 2 as was observed in a similar situation in an earlier work[5]. An antiferromagnetic coupling (energy of 22 meV) between Fe and Ni is observed in this case. (iii) Finally, a SW defect causes an antiferromagnetic exchange interaction of strength $\sim$14.8 meV between Fe and Ni. In this case, the spin state of Fe is retained as S = 1.

Due to complex structural changes, the electronic structures of Fe and Ni are expected to be modified significantly depending on the adsorption site. To make a comparison, we show in Fig. 2 the d-projected DOS of Fe in FeP and one of the selected Ni atoms of the Ni substrate for two cases: (a) Fe placed at the hexagonal site and (b) Fe placed on top of a divacancy site. For the hexagonal adsorption site, the d-DOS of Fe is very close to a S = 2 DOS of Fe in a gas-phase FeP molecule, indicating a very weak effect on the Fe DOS due to the presence of graphene and Ni. To elucidate this clearly, we have indicated the d_{z^2} dominated peaks in the Fe and Ni DOS, which do not display any significant hybridization between these states (Fig. 2). This is demonstrated by the absence of common features of the Fe and Ni projected states. On the contrary, for a divacancy site, Fe and Ni DOS are significantly modified with the presence of clearly hybridizing d_{z^2} states indicated by bars in Fig. 2, that coincide in energy. Also, one clearly observes localized d-states of the Ni atom surrounded by C atoms. As a result of the strong p-d hybridization between Ni and C states, the local magnetic moment of these Ni atoms is almost quenched. In this case, a direct bonding controls the exchange mechanism and FeP is antiferromagnetically coupled to Ni with a coupling strength of 22 meV.

We can now think of a situation where a graphene lattice grown on Ni possesses several types of defects, e.g., monovacancy, divacancy and SW. It should be noted that the defect formation energies (DFE) in free-standing graphene are much higher than for the situation of graphene deposited on a Ni(111) surface. Our calculated values of the DFE are 2.91 eV and 3.83 eV for a monovacancy and a divacancy defect in comparison to 7–8 eV for vacancy formation energies in a free-standing graphene. Therefore, the creation of these defects, either naturally or by an ion-irradiation experiment should be easier compared to free standing graphene. Molecules adsorbed on graphene with these defects introduced, are expected to produce different kinds of exchange coupling depending on specific defect sites.

Due to the presence of defects in graphene and the adsorbed FeP, the magnetic properties of the first Ni layer also change in a very interesting way. In Fig. 3, we show the change in the magnetic moments of the Ni atoms in the first layer when defects are present along with FeP, compared to the case with a pure graphene layer on the Ni substrate (indicated as m_0) as a function of the coordination shells around the region of the first layer where defects are present. For a pure graphene lattice deposited on Ni, the magnetic moments in the first Ni layers have a homogeneous pattern throughout the layer. In addition to that, the effect of adsorbed FeP on the first layer Ni moment is shown for the **Top-A** position, where a small modification of the moment is observed. However the most noticeable changes are seen in presence of defected graphene, where different types of non-monotonic variations depending on the type of defect are found. For example, the Ni atoms closest (in the first coordination shell) to monovacancy center lose around 0.15 μ_B whereas for distant shells, the moments increase by a smaller amount ($\sim$0.025 μ_B). The most interesting change is observed for the SW defect. In the first coordination shell, the Ni atoms lose around 0.075 μ_B whereas for the fifth shell, a large increase of about 0.2 μ_B is observed. Moreover, a gradual change in the moment is observed as a function of coordination shells with a changeover in sign in the

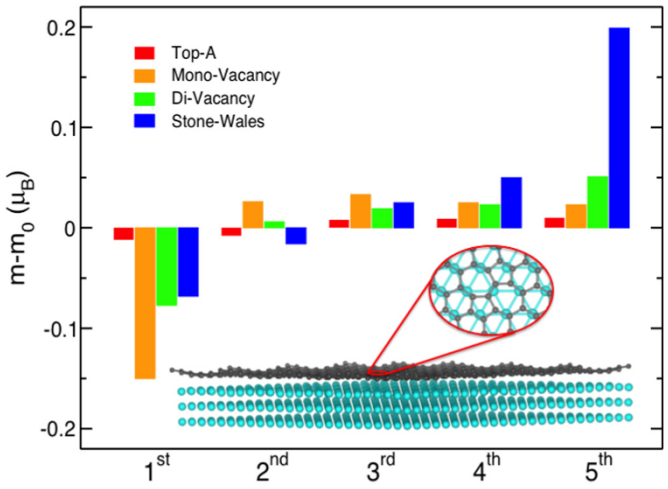

Figure 3 | Change in magnetic moments of Ni atoms in the first layer (averaged over moments in the respective coordination shells) between FeP/graphene/Ni with different types of defects as indicated and graphene/Ni without FeP and any defect in the graphene layer (moment indicated as m_0). The coordination shells are chosen around the defect centers above which the molecules are adsorbed. The first coordination shell includes the nearest neighbor atoms in a hexagonal cell (of Ni (111) surface). 2nd coordination shell consists of next nearest neighbors and so on. Atoms in the unit cell are considered only. An average moment in the respective coordination shell is shown. The shells are indicated in the x-axis label. Also, the optimized structure (side) of graphene with a SW defect on Ni is shown with an area zoomed around SW site. In the zoomed area, both graphene lattice with SW center (5577) and first layer of Ni surface are shown.

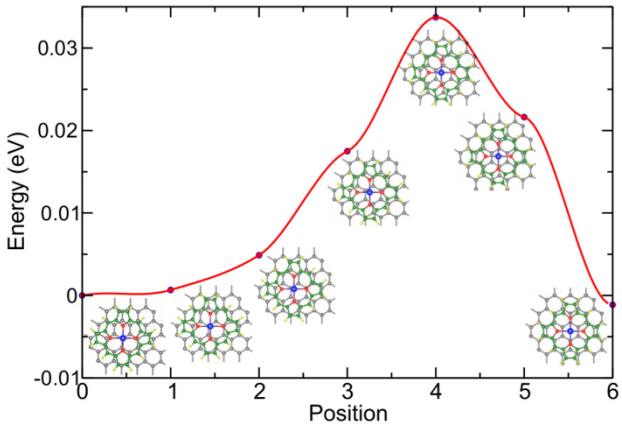

Figure 4 | Energy barrier calculated by NEB in moving FeP from a top-A to a neighboring hexagonal site on the graphene lattice adsorbed on Ni(111). For each position along the reaction coordinate, the optimized local structures of FeP and graphene lattice are shown.

third shell. It is observed that a SW defect causes a significant buckling in the graphene lattice and as a result, the distance between the buckled graphene sheet and the first Ni layer has a significant spatial variation, which leads to the variation in the local Ni moments. Therefore, one may conclude that the modifications of the first layer Ni moments affect the exchange interaction between Ni and Fe in FeP in different ways for different types of defects.

The next important question is whether the FeP molecules will overcome possible energy barriers, once adsorbed on graphene, so that they move to different adsorption sites with comparable energies. In order to investigate this, we have performed nudged elastic band (NEB) calculations to determine the energy barrier in moving an FeP molecule between a hexagonal site to a **Top-A** site on a defect free graphene lattice. We have chosen the **Top-A** site as it is only 2 meV higher in energy than the hexagonal site. A defect-free graphene is intentionally chosen as the adsorption on a defected graphene is expected to be stronger[5,16,17] and hence, the transition barrier is expected to be higher. Therefore our calculated value for a defect-free graphene sets the lower limit for the diffusion barrier. The calculated energy barrier is 33 meV as observed in Fig. 4. This indicates that FeP can diffuse from the **hexagonal** ground state adsorption site to the next energetically available **Top-A** site at the room temperature or slightly above it. However, one can control this diffusion by adjusting the temperature. In Fig. 4, the geometries of FeP and a part of the underlying graphene lattice are presented along the reaction path. One may conclude that FeP molecules will remain locked due to the energy barrier, at their respective adsorption sites with well-defined spin states and exchange coupling with underlying Ni substrate. One may envisage controlled formation of specific types of defects and achieving either parallel or antiparallel orientation of Fe moments relative to the moments in the Ni layers.

We should point out that one may reach metastable solutions for these systems. Therefore, we have considered several starting possibilities (both in structure and spin state) for each adsorption geometry to reach the true ground state. Most importantly, spin switching (S = 1 to S = 2) has been observed for FeP adsorbed on the **Hexagonal** and **divacancy** adsorption sites. On the divacancy site, a high spin S = 2 solution is always obtained. S = 1 and S = 2 spin states are very close in energy for the **Hexagonal** and **SW** sites. For **SW**, an AFM ground state is found with S = 1 while a FM S = 2 spin state is 6 meV higher in energy. For the **Hexagonal** site, S = 2 spin state is found to be the ground state with degenerate FM and AFM solutions. However, a S = 1 spin state could be stabilized at 24 meV higher energy. For other adsorptions sites, a stable S = 1 spin state is always found.

Magnetic anisotropy and spin dipole moment. So far, organometallic complexes have been successfully deposited[18] on nonmagnetic (e.g., Cu, Au, Ag etc.) and magnetic surfaces (e.g., Co, Ni etc.). The magnetic ordering between the molecular spins has been realized either by exchange coupling with the magnetic substrates or by externally applied magnetic field. As thermal fluctuations are always detrimental towards the magnetic ordering, the strength of molecular magnetic anisotropy stands as an important issue. In organic molecules with a transition metal atom center, the ligand field splitting is 2–3 order larger compared to the spin-orbit coupling. A perturbative approach thus can safely be considered to calculate the magnetocrystalline anisotropy energy. The leading contribution comes from the second order term while higher order terms can be neglected.

The magnetocrystalline anisotropy originates from coupling between lattice and spin, which can be expressed as:

$$H_{SO} = \zeta(r)\mathrm{L.S} = \zeta(r)\left(L_x S_x + L_y S_y + L_z S_z\right) \quad (1)$$

where H_{SO} is the spin-orbit coupling hamiltonian and ζ is the spin orbit coupling constant defined as $\zeta = \langle\zeta(r)\rangle = \int R_{3d}^2(r)\zeta(r)r^2dr$, $R_{3d}(r)$ being the radial part of the 3d wave function. The value of ζ for Fe^{2+} has been considered as 0.049 eV[19], taken from the literature. Spin-orbit contribution to the energy derived from second order perturbation theory reads as:

$$E_{SO} = -\zeta^2 \sum_{u,o} \frac{[\langle u|\mathrm{L.S}|o\rangle\ \langle o|\mathrm{L.S}|u\rangle]}{E_u - E_o} \quad (2)$$

Here $|o\rangle$ and $|u\rangle$ correspond to occupied and unoccupied states weighted by the occupations of the Fe-d orbitals. $|u/o\rangle = |lm, \sigma\rangle$, L and S denote orbital and spin operators and E_u and E_o denote

eigenvalues of unoccupied and occupied states, which are obtained from ab initio calculations. As the denominator decreases, spin-orbit coupling energy contribution increases. The relative arrangement of Fe-d orbitals is thus very important and can be affected by the adsorption site. Our calculated magnetic anisotropy energies are presented in Table I. A plus (minus) sign of MAE corresponds to an in-plane (out-of-plane) easy axis of magnetization.

One of the most relevant properties for magnetic nanosystems is the magnetic dipole contribution $\langle T_z \rangle$ as it can have a very large value for low dimensional structures, as reported earlier for clusters[20] and organometallics[5,21]. This has a significant contribution in the effective spin moment, $S_{eff} = M_s + 7\langle T_z \rangle$, which is measured in XMCD experiments, M_s being the saturation spin moment. It should be noted that the sign of $\langle T_z \rangle$ can even be opposite to the spin moment giving rise to a small value of the effective spin moment[5]. We have calculated spin dipole contribution following the formalism prescribed in the literature[22–24] and the results are shown in Table I. Due to different adsorption sites, ligand field splittings are different and spin densities have different kinds of asphericities. All these are counted in the spin dipole contribution as this measures the asphericity in the spin density. As a result, the effective spin moments are significantly different for different adsorption sites, which should be captured in XMCD measurements.

All the above discussions lead to the exploration of possible applications of defect controlled magnetism in molecular nanospintronics. Single-molecule magnets have been proposed to act as robust spin qubits[25]. The stability of these nanomagnets is dictated by the magnetic anisotropy[26]. According to our study, one can achieve a rational design of spatially distributed single molecule nanomagnets by selectively producing relevant point defects on the graphene sheet with the help of focussed ion-beam technique. As a consequence, the relative orientation of molecular spins in individual nanomagnets at designated lattice sites will provide the possibility of achieving robust spin qubits to be used in spin logic operations.

Discussion

Our ab initio density functional calculations suggest that a graphene layer without structural defects placed in between an FeP molecule and a ferromagnetic Ni substrate decouples the molecule-substrate magnetic interaction for the most favorable hexagonal adsorption site. However, point defects in the graphene lattice can mediate ferromagnetic or antiferromagnetic coupling depending on the nature of the defect. This complex behavior of exchange interactions is related to the magnetization profile in the defected graphene lattice induced by the underlying Ni substrate. A long-ranged ferrimagnetic sublattice magnetization in defect free graphene is drastically modified by the introduction of defects and hence, different types of magnetic coupling are observed depending on the adsorption site on graphene and also the type of defect in graphene. Not only the magnetic coupling but a strong variation in magnetic anisotropy energies and easy axes of magnetization is observed along with large contributions from spin-dipolar interaction. We propose that the control over the spin of single molecule magnets, e.g., FeP by selective defect production in graphene may lead to robust spin qubits for spin logic operations. We hope that our prediction of defect controlled magnetism will boost the experimental verifications with the help of controlled defect productions by ion-irradiation techniques and magnetic measurements by XMCD experiments.

Table I | Magnetic anisotropy energies and spin-dipole moments of Fe in FeP on different adsorption sites. The −ve (+ve) sign indicates out-of-plane (in-plane) easy axis of magnetization of Fe moment in FeP

Adsorption site	MAE (meV)	$7\langle T_z \rangle (\mu_B)$
TOP-A	−0.087	−2.07
TOP-B	−0.052	−1.99
Hexagon	0.608	1.55
Divacancy	−0.245	−1.53
Monovacancy	−0.096	−2.05
SW	−0.099	−2.08

Methods

We have performed first-principles calculations based on density functional theory with a full potential plane wave based code VASP[27,28]. The Ni(111) surface is considered as the substrate, as graphene can easily be grown on top of it due to excellent lattice matching. A slab of three Ni layers consisting of 108 atoms has been considered along with a graphene monolayer with 72 atoms (6 × 6 supercell) on top of the metallic slab. The size of the supercell is chosen in such a way that the magnetic centers of FeP are at least 15 Å apart from each other in the lateral direction, which minimizes the interaction among them. FeP with an Fe center consists of 37 atoms, yielding a total of 217 atoms in the simulation cell. A 3 × 3 × 1 k-point mesh is chosen for geometry optimizations with a force tolerance of 0.01 eV/Å. All the atomic positions were relaxed except the ones in the lowest Ni-layer, which is fixed to have the in-plane lattice constant as that of bulk Ni. A 4 × 4 × 2 k-point mesh is considered for calculating total energies and other properties. We have employed PBE + U approach within Hubbard model[29] to incorporate strong Coulomb interaction with the Coulomb parameter U and exchange parameter J fixed as 4 and 1 eV respectively for Fe d-orbitals. These parameters have been shown[30] to reproduce certain experimental results. It should be mentioned that the choice of U and J may have important consequences in the properties of materials[31]. These parameters have been explicitly calculated by first principles and the results have been successfully compared to experiments in some cases[32–34]. In the present context, the value of U calculated by linear response method by Scherlis *et al*[35]. for heme is around 4 eV and hence justifies our choice of U. All the calculations are performed including an empirical form of dispersion correction given by Grimme[36]. The inclusion of van der Waals interaction is crucial due to the presence of π-π interactions between FeP and graphene. Also, it becomes very important in describing the binding characteristics between graphene and Ni[15].

1. Wende, H. *et al*. Substrate-induced magnetic ordering and switching of iron porphyrin molecules. *Nat. Mater.* **6**, 516–520 (2007).
2. Dediu, V. A., Hueso, L. E. & Taliani, C. Spin routes in organic semiconductors. *Nature Mater.* **8**, 707–716 (2009).
3. Leoni, T. *et al*. Controlling the Charge State of a Single Redox Molecular Switch. *Phys. Rev. Lett.* **106**, 216103 (2011).
4. Bhandary, S. *et al*. Manipulation of spin state of iron porphyrin by chemisorption on magnetic substrates. *Phys. Rev. B* **88**, 024401 (2013).
5. Bhandary, S. *et al*. Graphene as a Reversible Spin Manipulator of Molecular Magnets. *Phys. Rev. Lett.* **107**, 257202 (2011).
6. Geim, A. K. & Novoselov, K. S. The rise of graphene. *Nature Mater.* **6**, 183–191 (2007).
7. Castro Neto, A. H., Guinea, F., Peres, N. M., Novoselov, K. S. & Geim, A. K. The electronic properties of graphene. *Rev. Mod. Phys.* **81**, 109–162 (2009).
8. Geim, A. K. Graphene: Status and Prospects *Science* **324**, 1530–1534 (2009).
9. Yazyev, O. V. Emergence of magnetism in graphene materials and nanostructures. *Rep. Prog. Phys.* **73**, 056501 (2010).
10. Weser, M. *et al*. Induced magnetism of carbon atoms at the graphene/Ni(111) interface. *Appl. Phys. Lett.* **96**, 012504 (2010).
11. Gass, M. H. *et al*. Free-standing graphene at atomic resolution. *Nat. Nanotech.* **3**, 676–681 (2008).
12. Hashimoto, A., Suenaga, K., Gloter, A., Urita, K. & Iijima, S. Direct evidence for atomic defects in graphene layers. *Nature* **430**, 870–873 (2004).
13. Ugeda, M. M. *et al*. Electronic and structural characterization of divacancies in irradiated graphene. *Phys. Rev. B* **85**, 121402(R) (2012).
14. Meyer, J. C. *et al*. Direct Imaging of Lattice Atoms and Topological Defects in Graphene Membranes. *Nano Lett.* **8**, 3582–3586 (2008).
15. Mittendorfer, F. *et al*. Graphene on Ni(111): Strong interaction and weak adsorption. *Phys. Rev. B* **84**, 201401(R) (2011).
16. Hajati, Y. *et al*. Improved gas sensing activity in structurally defected bilayer graphene. *Nanotechnology* **23**, 505501 (2012).
17. Sanyal, B., Eriksson, O., Jansson, U. & Grennberg, H. Molecular adsorption in graphene with divacancy defects. *Phys. Rev. B* **79**, 113409 (2009).
18. Miller, C. W. *et al*. Quantitative structural analysis of organic thin films: An x-ray diffraction study. *Phys. Rev. B* **72**, 104113 (2005).
19. Cole, G. M. & Garrett, B. B. Atomic and Molecular Spin-Orbit Coupling Constants for 3d Transition Metal Ions. *Inorg. Chem.* **9**, 1898–1902 (1970).
20. Sipr, O., Minar, J. & Ebert, H. On the importance of the magnetic dipole term T_z in analyzing X-ray magnetic circular dichroism spectra of clusters. *Eur. Phys. Lett.* **87**, 67007 (2007).
21. Stepanow, S. *et al*. Spin and Orbital Magnetic Moment Anisotropies of Monodispersed Bis(Phthalocyaninato)Terbium on a Copper Surface. *JACS Comm.* **132**, 11900–11901 (2010).

22. Wu, R. & Freeman, A. J. Limitation of the Magnetic-Circular-Dichroism Spin Sum Rule for Transition Metals and Importance of the Magnetic Dipole Term. *Phys. Rev. Lett.* **73**, 1994 (1994).
23. Stöhr, J. & König, H. Determination of Spin- and Orbital-Moment Anisotropies in Transition Metals by Angle-Dependent X-Ray Magnetic Circular Dichroism. *Phys. Rev. Lett.* **75**, 3748 (1995).
24. Oguchi, T. & Shishidou, T. Anisotropic property of magnetic dipole in bulk, surface, and overlayer systems. *Phys. Rev. B* **70**, 024412 (2004).
25. Baldovi, J. J. *et al*. Rational Design of Single-Ion Magnets and Spin Qubits Based on Mononuclear Lanthanoid Complexes. *Inorg. Chem.* **51**, 12565–12574 (2012).
26. G-Coca, S., Cremades, E., A-Alcalde, N. & Ruiz, E. Mononuclear Single-Molecule Magnets: Tailoring the Magnetic Anisotropy of First-Row Transition-Metal Complexes. *JACS* **135**, 7010–7018 (2013).
27. Kresse, G. & Hafner, J. Ab initio molecular dynamics for liquid metals. *Phys. Rev. B* **47**, R558 (1993).
28. Kresse, G. & Furthmüller, J. Efficient iterative schemes for ab initio total-energy calculations using a plane-wave basis set. *Phys. Rev. B* **54**, 11169 (1996).
29. Anisimov, V. I., Aryasetiawan, F. & Lichtenstein, A. I. First-principles calculations of the electronic structure and spectra of strongly correlated systems: the LDA + U method. *J. Phys.:Condens. Matter* **9**, 767–808 (1997).
30. Panchmatia, P. M., Sanyal, B. & Oppeneer, P. M. GGA + U modeling of structural, electronic, and magnetic properties of iron porphyrin-type molecules. *Chem. Phys.* **343**, 47–60 (2008).
31. Rondinelli, J. M. & Spaldin, N. A. Structural effects on the spin-state transition in epitaxially strained LaCoO3 films. *Phys. Rev. B* **79**, 054409 (2009).
32. Hsu, H., Blaha, P., Cococcioni, M. & Wentzcovitch, R. M. Spin-state crossover and hyperfine interactions of ferric iron in $MgSiO_3$ perovskite. *Phys. Rev. Lett.* **106**, 118501 (2011).
33. Kulik, H. J., Cococcioni, M., Scherlis, D. A. & Marzari, N. Density functional theory in transition-metal chemistry: A self-consistent Hubbard U approach. *Phys. Rev. Lett.* **97**, 103001 (2006).
34. Himmetoglu, B., Wentzcovitch, R. M. & Cococcioni, M. First-principles study of electronic and structural properties of CuO. *Phys. Rev. B* **84**, 115108 (2011).
35. Scherlis, D. A., Cococcioni, M., Sit, P. & Marzari, N. Simulation of heme using DFT + U: A step toward accurate spin-state energetics. *J. Phys. Chem. B* **111**, 7384–7391 (2007).
36. Grimme, S. Semiempirical GGA-type density functional constructed with a long-range dispersion correction. *J. Comp Chem.* **27**, 1787–1799 (2006).

Acknowledgments

We thank Oscar Grånäs for useful discussions. B.S. acknowledges Carl Tryggers Stiftelse and VR/SIDA for financial support. O.E. is in addition grateful to the KAW foundation, eSSENCE and the ERC(project 247062 - ASD) for support. We also acknowledge SNIC-UPPMAX, SNIC-HPC2N and SNIC-NSC centers under the Swedish National Infrastructure for Computing (SNIC) resources for the allocation of time in high performance supercomputers.

Author contributions

B.S. designed the project and S.B. carried out the calculations. S.B., O.E. and B.S. analyzed the data and wrote the paper.

Additional information

Competing financial interests: The authors declare no competing financial interests.

How to cite this article: Bhandary, S., Eriksson, O. & Sanyal, B. Defect controlled magnetism in FeP/graphene/Ni(111). *Sci. Rep.* **3**, 3405; DOI:10.1038/srep03405 (2013).